

## LOW TEMPERATURE FORMATION OF NITROGEN-SUBSTITUTED POLYCYCLIC AROMATIC HYDROCARBONS (PANHs)—BARRIERLESS ROUTES TO DIHYDRO(iso)QUINOLINES

DORIAN S. N. PARKER<sup>1</sup>, TAO YANG<sup>1</sup>, BENI B. DANGI<sup>1</sup>, RALF I. KAISER<sup>1</sup>, PARTHA P. BERA<sup>2,3</sup>, AND TIMOTHY J. LEE<sup>2</sup>

<sup>1</sup>Department of Chemistry, University of Hawaii at Manoa, Honolulu, HI 96822, USA; ralfk@hawaii.edu

<sup>2</sup>Space Science and Astrobiology Division, NASA Ames Research Center, Moffett Field, Mountain View, CA 94035, USA; Timothy.J.Lee@nasa.gov

<sup>3</sup>Bay Area Environmental Research Institute, 625 2nd St Ste. 209, Petaluma, CA 94952, USA

Received 2015 September 3; accepted 2015 October 24; published 2015 December 16

### ABSTRACT

Meteorites contain bio-relevant molecules such as vitamins and nucleobases, which consist of aromatic structures with embedded nitrogen atoms. Questions remain over the chemical mechanisms responsible for the formation of nitrogen-substituted polycyclic aromatic hydrocarbons (PANHs) in extraterrestrial environments. By exploiting single collision conditions, we show that a radical mediated bimolecular collision between pyridyl radicals and 1,3-butadiene in the gas phase forms nitrogen-substituted polycyclic aromatic hydrocarbons (PANHs) 1,4-dihydroquinoline and to a minor amount 1,4-dihydroisoquinoline. The reaction proceeds through the formation of a van der Waals complex, which circumnavigates the entrance barrier implying it can operate at very low kinetic energy and therefore at low temperatures of 10 K as present in cold molecular clouds such as TMC-1. The discovery of facile de facto barrierless exoergic reaction mechanisms leading to PANH formation could play an important role in providing a population of aromatic structures upon which further photo-processing of ice condensates could occur to form nucleobases.

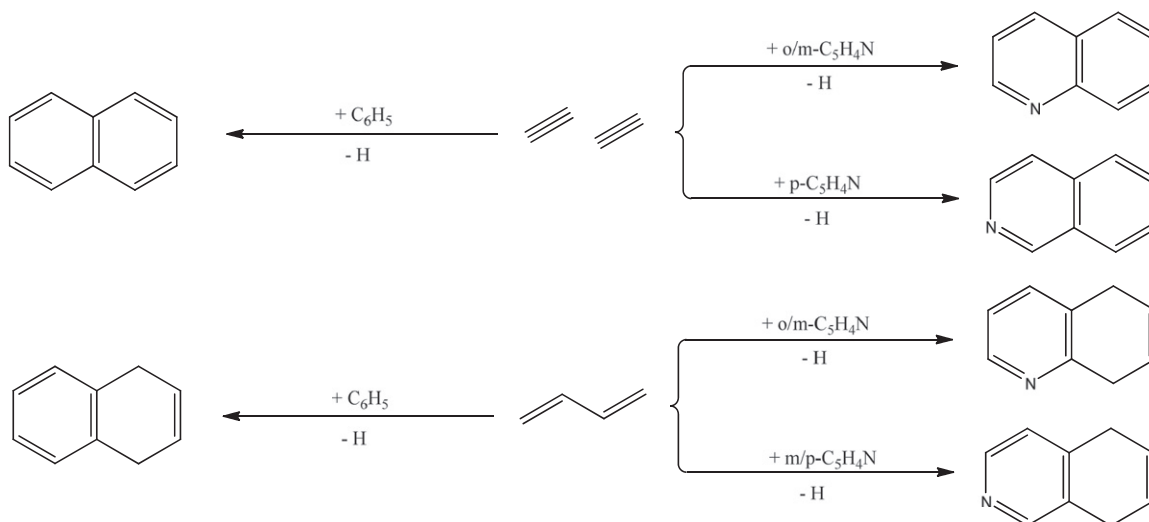
*Key words:* astrobiology – astrochemistry – ISM: molecules – molecular processes

### 1. INTRODUCTION

Since the discovery of biorelevant molecules such as vitamin B3 (niacin; Smith et al. 2014) and nucleobases (pyrimidines, purines; Martins et al. 2008; Callahan et al. 2011) in carbonaceous chondrites like Murchison, questions remain over their formation routes in extraterrestrial environments. The detection of terrestrially rare nucleobases 2,6-diaminopurine and 6,8-diaminopurine in the Murchison meteorite (Robins 1958; Callahan et al. 2011) together with an <sup>15</sup>N/<sup>14</sup>N isotope enrichment suggest an interstellar origin (Pizzarello & Holmes 2009). However, well defined formation routes of these molecules are still lacking. Their related compounds—polycyclic aromatic hydrocarbons (PAHs) along with their cations and (partially) hydrogenated PAHs—have been proposed to be linked to the synthesis of these biorelevant molecules in the interstellar medium (ISM); strong infrared emission bands observed at 3.3, 6.2, 7.7, 11.2, and 12.7  $\mu\text{m}$  have been attributed to ultraviolet pumped infrared fluorescence by a population of PAHs with more than 50 carbon atoms (Tielens 2008). The 6.2  $\mu\text{m}$  band has been linked to protonated PAHs (Knorke et al. 2009; Ricks et al. 2009), but might also be the result of nitrogen-substituted PAHs (Hudgins et al. 2005). Calculations suggest that up to 10% of the carbon budget of the ISM could be tied up in large aromatic structures, likely with a proportion carrying embedded nitrogen atoms in the gas phase PAHs (Puget & Leger 1989; Ehrenfreund & Sephton 2006; Tielens 2008; Herbst & van Dishoeck 2009). Recent laboratory simulations of the photo processing of interstellar ice analog samples suggest that nucleobases might be formed (Bernstein et al. 1999; Nuevo et al. 2009, 2014). However, detailed reaction pathways to these molecules have remained conjecture on the molecular level since the nitrogen-bearing molecules were only inferred tentatively after dissolving organic residues produced in the photolysis followed by a gas chromatography—mass spectrometry separation of the hydrolyzed residues.

An alternative reaction mechanism has recently been proposed in which nitrogen atoms are incorporated within a bicyclic aromatic system through a series of radical-mediated gas phase reactions (Parker et al. 2015). Here, (iso)quinoline (C<sub>9</sub>H<sub>7</sub>N; Scheme 1) was shown to be formed through the hydrogen-abstraction acetylene-addition (HACA) pathway involving pyridyl radicals (C<sub>5</sub>H<sub>4</sub>N) and acetylene (C<sub>2</sub>H<sub>2</sub>) at elevated temperatures of up to 1500 K. Nitrogen atom incorporation has been shown to occur in mono and bicyclic six-membered carbon rings via ion-molecule reactions (Hamid et al. 2014a, 2014b), however, not via bimolecular reactions under single collision conditions as is characteristic for cold molecular clouds. Current models of circumstellar envelopes of dying carbon stars propose a versatile and robust environment in which small unsaturated molecules and their radicals undergo a series of radical-mediated cyclization reactions leading to (N)PAHs (Ziurys 2006; Cherchneff 2011). These mechanisms, borrowed from the combustion community, have often implied high temperature environments to operate due to intrinsic entrance barriers to reaction. However, recent experiments under single collision conditions combined with electronic structure calculations indicate that this is not always the case. If a phenyl-type radical such as phenyl or an alkyl-substituted phenyl radical reacts with a C4 to C5 hydrocarbon and a resonantly stabilized free radical (RSFR) intermediate is formed, the addition is de facto barrierless and proceeds via a submerged barrier; hence PAH formation can also operate in cold molecular clouds at temperatures as low as 10 K (Kaiser et al. 2012, 2015; Parker et al. 2012a, 2012b, 2014b, 2014c; Golan et al. 2013; Dangi et al. 2014).

In the present combined experimental and computational work, we transfer the principles of low temperature aromatization and PAH formation to the synthesis of prototypical nitrogen substituted polycyclic aromatic hydrocarbons (PANHs) belonging to the dihydro(iso)quinoline family (C<sub>9</sub>H<sub>9</sub>N) as detected in the Murchison meteorite (Plows



**Scheme 1.** Top: formation pathways to naphthalene as well as (iso)quinoline via HACA-type pathways at elevated temperatures (Parker et al. 2012a, 2015). Bottom: formation routes to 1,4-dihydroquinoline, 1,4-dihydroquinoline, and 1,4-dihydroisoquinoline through the reaction of phenyl and pyridyl radicals plus 1,3-butadiene, respectively (Kaiser et al. 2012).

et al. 2003). Here, these molecules are formed through the reaction of aromatic nitrogen-bearing radicals—ortho- and meta-pyridyl (C<sub>5</sub>H<sub>4</sub>N)—with 1,3-butadiene (C<sub>4</sub>H<sub>6</sub>; Scheme 1). In combination with electronic structure calculations, we reveal that the formation of dihydro(iso)quinolines (C<sub>9</sub>H<sub>9</sub>N) proceeds via barrier-less addition and isomerization eventually leading to aromatization and formation of dihydro(iso)quinolines (C<sub>9</sub>H<sub>9</sub>N) plus a hydrogen atom. The facile synthesis of dihydro(iso)quinolines and potentially more complex PANHs in ultra-low temperature environments represents a hitherto overlooked route to a key class of bio-relevant molecules—PANHs—in the gas phase of the ISM.

## 2. EXPERIMENTAL

The elementary reactions of the meta-pyridyl (*m*-C<sub>5</sub>H<sub>4</sub>N; X<sup>2</sup>A<sub>1</sub>) and ortho-pyridyl (*o*-C<sub>5</sub>H<sub>4</sub>N; X<sup>2</sup>A<sub>1</sub>) radicals with 1,3-butadiene (C<sub>4</sub>H<sub>6</sub>, X<sup>1</sup>A<sub>g</sub>) were carried out utilizing a universal crossed molecular beams machine at The University of Hawaii (Kaiser et al. 1997, 1999a, 1999b, 2001, 2003, 2010; Balucani et al. 2001, 2002; Stahl et al. 2002). In the primary source chamber, supersonic molecular beams of the pyridyl radicals were formed via photolysis of helium-seeded meta-chloropyridine (C<sub>5</sub>H<sub>4</sub>NCl, Aldrich)/ortho-chloropyridine (C<sub>5</sub>H<sub>4</sub>NCl, Aldrich) at fractions of 0.1% by bubbling helium (99.9999%; Gaspro) at pressures of 1300 Torr through ortho-/meta-chloropyridine in a bubbler at 293 K. The molecular beam was then introduced into the primary chamber by a Proch-Trickl pulsed valve with repetition rates of 120 Hz and 80 μs opening time. The precursors were photolyzed 1 mm downstream of the nozzle at 12 mJ per pulse (193 nm). A four slot chopper placed after the skimmer selected a section of the pyridyl radical beam at collision energies of 48–50 kJ mol<sup>-1</sup> (Table 1). This part of the radical beam perpendicularly crossed a pulsed molecular beam of 1,3-butadiene (Table 1). The products were detected exploiting a triply differentially pumped quadrupole mass spectrometer in time-of-flight (TOF) mode after electron-impact ionization of the neutral species. The TOF spectra of the reactively scattered products were taken at distinct laboratory angles within the scattering plane. The experimental data were transformed via a forward-convolution

**Table 1**

Molecular Beam Characteristics: Peak Velocity ( $v_p$  (m s<sup>-1</sup>)), Speed Ratio ( $S$ ), Collision Energy  $E_{col}$  (kJ mol<sup>-1</sup>), and Center-of-mass Angle  $\Theta_{CM}$

	$v_p$ (m s <sup>-1</sup> )	$S$	$E_{col}$ (kJ mol <sup>-1</sup> )	$\Theta_{CM}$
1,3-butadiene	740 ± 20	8.0 ± 1.5	...	...
meta-pyridyl	1600 ± 21	12.0 ± 2.6	48.6 ± 2.4	17.6 ± 1.4
ortho-pyridyl	1632 ± 32	10.0 ± 3.6	50.3 ± 3.8	17.3 ± 1.6

routine (Vernon 1981; Weiss 1986) into the center-of-mass (CM) frame. This procedure results in the angular flux distribution,  $T(\theta)$ , and the translational energy flux distribution,  $P(E_T)$ , in the CM frame, which are adjusted to fit the experimental data (TOF spectra and the laboratory angular distributions). The CM functions deliver information on the reaction dynamics and reaction energy. We would like to point out that para-pyridyl radicals could not be generated due to the lack of commercially available precursor molecules such as para-chloro pyridine.

## 3. THEORETICAL METHODS

We explored the potential energy surfaces (PESs) of the reaction of 1,3-butadiene with ortho-, meta-, and para-pyridyl radicals using ab initio coupled cluster and density functional theory methods. First, we identified all of the stationary points on the PESs along the reaction paths by full geometric optimization using Becke’s three-parameter exchange (B3; Becke 1993) functional along with the correlation functional of Lee, Yang, and Parr (LYP; Lee et al. 1988), and Pople’s split valence basis set 6-311+G\*. We then performed harmonic vibrational frequency calculations to ascertain the nature of minima and transition states. We refined the energies, at the B3LYP/6-311+G\* optimized geometries, by doing coupled cluster singles and doubles with perturbative triples [CCSD(T)] (Raghavachari et al. 1989) energy calculations along with a 6-311+G(2d,2p) (Clark et al. 1983; Frisch et al. 1984) basis set. 6-311+G(2d,2p) includes one set of diffuse functions on heavy atoms, and polarization functions, and adds up to a total of 360 basis functions for all of the intermediates and transition states that have 20 atoms each. Mindful of the well-known

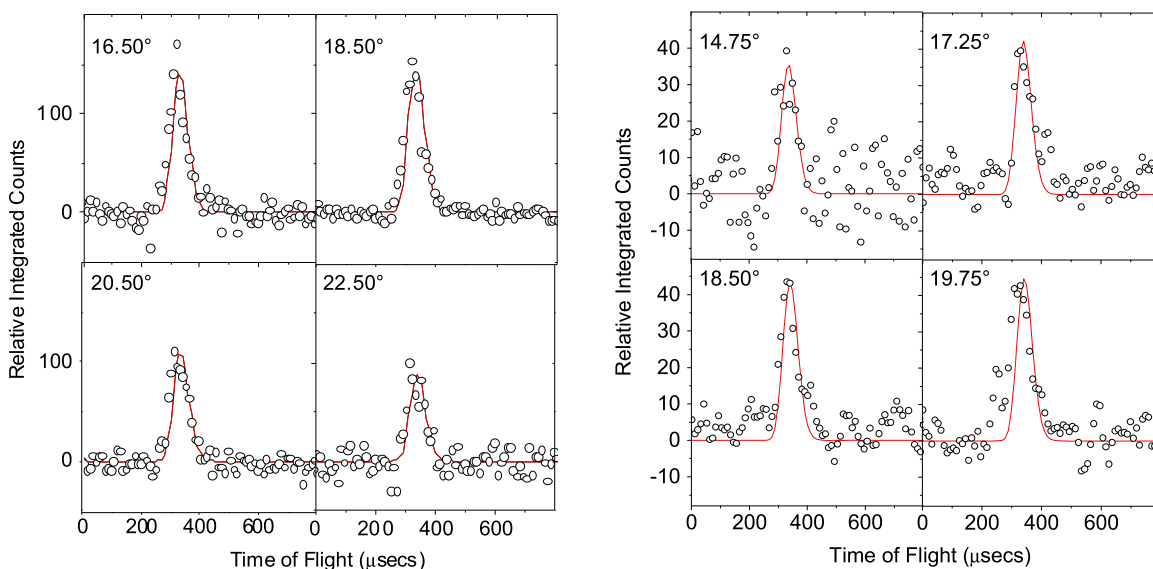


**Figure 1.** Selected TOF spectra recorded at  $m/z = 131$  ( $C_9H_9N^+$ ) at various laboratory angles for the reaction of the meta-pyridyl radical with 1,3-butadiene at a collision energy of  $48.6 \text{ kJ mol}^{-1}$  (left) and the ortho-pyridyl radical with 1,3-butadiene at a collision energy of  $50.3 \text{ kJ mol}^{-1}$ . The circles indicate the experimental data, and the solid lines indicate the calculated fits.

deficiency of the widely used B3LYP functional to predict the barrier heights (Lynch & Truhlar 2001) and long-range van der Waal’s type interactions, we treated the sigma complexes, and associated transition states, on the entrance channel of each of the three reactions with special care. We optimized these geometries using  $\omega$ B97X (Chai & Head-Gordon 2008) a range-separated density functional designed especially for these types of weakly interacting complexes, along with the 6-311+G\* basis set. The  $\omega$ B97X functional performs very well in predicting the binding energies and geometries of the van der Waal’s complexes (Witte et al. 2015). All B3LYP and  $\omega$ B97X calculations were done using the Q-Chem 3.2 quantum chemistry code (Shao et al. 2006), and the coupled cluster calculations were performed using the MOLPRO package (Werner & Knowles 2008). Finally, we computed the unimolecular rate constants under single collision conditions using the RRKM theory (Steinfeld et al. 1989) as implemented by Kislov et al. (2004). Using these unimolecular rate constants, we solved the rate equations to predict the product branching ratios for the first order decomposition of activated initial van der Waals complexes.

## 4. RESULTS

### 4.1. Crossed Molecule Beams Studies: Laboratory Frame

To investigate the reaction of pyridyl radicals with 1,3-butadiene, two systems were studied under single collision conditions: *m*-pyridyl ( $C_5H_4N$ ) and *o*-pyridyl ( $C_5H_4N$ ) plus 1,3-butadiene ( $C_4H_6$ ). In the reaction of *m*-pyridyl ( $C_5H_4N$ ; 78 amu) and *o*-pyridyl ( $C_5H_4N$ ; 78 amu) with 1,3-butadiene ( $C_4H_6$ ; 54 amu), the reactive scattering signal was monitored at a mass-to-charge ratio ( $m/z$ ) of 131 amu ( $C_9H_9N^+$ ). This finding suggests that the reaction proceeds by hydrogen atom (1 amu) ejection via a *m*-/*o*-pyridyl radical versus a hydrogen atom exchange pathway. It should be noted that the signal for both reactions was also observed at mass-to-charge ratios lower by 1 amu and 2 amu compared to the reactive scattering signal of the parent; these TOFs were superimposable after scaling with the TOFs recorded at  $C_9H_9N^+$ , and are therefore assigned

to dissociative electron impact ionization of the parents in the electron impact ionizer. We were unable to detect within the signal-to-noise limits of our experiments any  $C_9H_{10}N$  adducts (132 amu). Although both the *m*-pyridyl ( $C_5H_4N$ ) and *o*-pyridyl ( $C_5H_4N$ ) radical beams have similar number densities in the interaction region of the scattering chamber of a few  $10^{13}$  radicals  $\text{cm}^{-3}$ , the reactive scattering signal of the *m*-pyridyl radical is significantly stronger compared to the *o*-pyridyl radical by a factor of about 10 implying that the *m*-pyridyl radical is more reactive than the *o*-pyridyl with respect to product formation at  $m/z = 131$  amu ( $C_9H_9N^+$ ). Figures 1(a) and (b) depict selected time-of-flight (TOF) spectra recorded at  $m/z = 131$  ( $C_9H_9N^+$ ), each fit with a single channel. The reactive scattering signal shown in Figures 1(a) and (b) represents the synthesis of a product with the molecular formula  $C_9H_9N$  formed by the reaction of the meta-pyridyl and ortho-pyridyl radical with 1,3-butadiene and ejection of a hydrogen atom under single collision conditions. The laboratory angular distributions for each reaction are shown in Figures 2(a) and (b), respectively. These laboratory angular distributions are nearly symmetric around the CM angles of  $17.6 \pm 1.2^\circ$  and  $17.3 \pm 1.2^\circ$ ; this finding is evidence of indirect scattering dynamics via complex formation ( $C_9H_{10}N$ ). The larger error bars of the *o*-pyridyl—1,3-butadiene system are the results of the lower intensity of the reactive scattering signal at  $m/z = 131$  as discussed above.

### 4.2. Crossed Molecule Beams Studies: CM Frame

Having established that the products formed in the reactions of both the *o*- and *m*-pyridyl radical with 1,3-butadiene have the molecular formula  $C_9H_9N$  (131 amu), we attempt now to elucidate the underlying reaction dynamics by converting the laboratory data to the CM reference frame. This results in the CM translational energy ( $P(E_T)$ ) and angular ( $T(\theta)$ ) distributions (Figure 3). In both reactions, the laboratory data could be reproduced with a single channel indicating that the reaction of pyridyl (78 amu) with 1,3-butadiene (54 amu) yields  $C_9H_9N$  (131 amu) plus atomic hydrogen (1 amu). The CM functions in

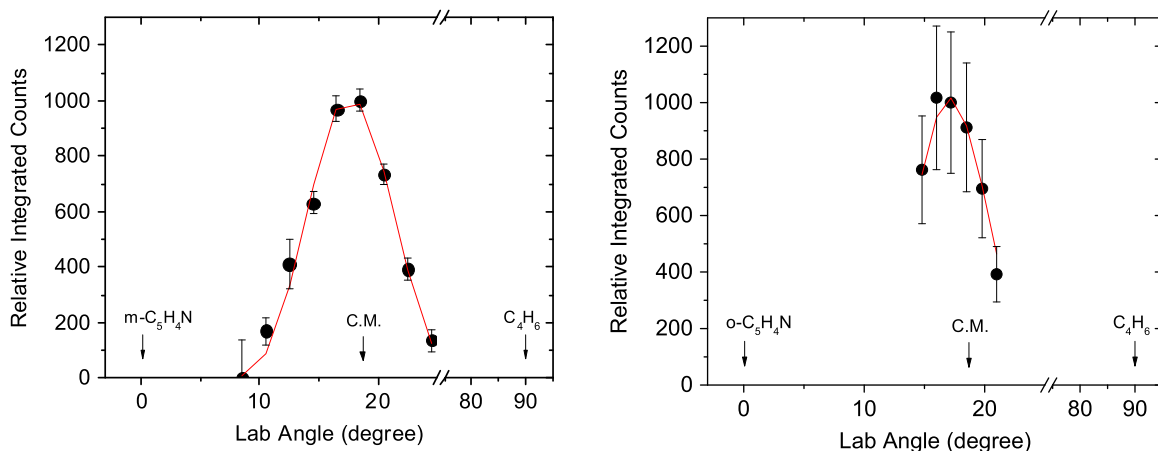


**Figure 2.** Laboratory angular distribution (LAB) of the  $C_9H_9N$  product recorded at  $m/z = 131$  ( $C_9H_9N^+$ ) for the reaction of the meta-pyridyl radical with 1,3-butadiene at a collision energy of  $48.6 \text{ kJ mol}^{-1}$  (left) and the ortho-pyridyl radical with 1,3-butadiene at a collision energy of  $50.3 \text{ kJ mol}^{-1}$ . Circles and error bars indicate experimental data, and the solid line indicates the calculated distribution with the one channel best-fit CM functions. Up to  $10^7$  TOFs were taken at each angle.

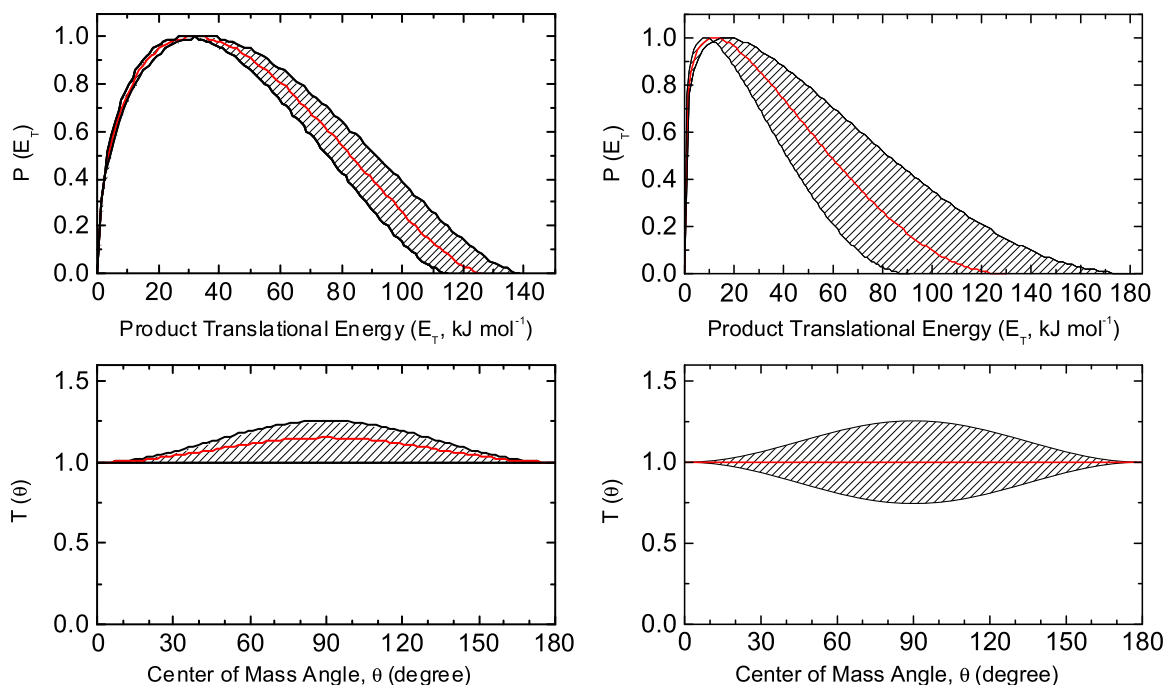


**Figure 3.** Center-of-mass angular (top) and translational energy flux distributions (bottom) leading to the formation of dihydroquinoline ( $C_9H_9N$ ) isomers plus atomic hydrogen in the reaction of the meta-pyridyl radical with 1,3-butadiene (left) and the ortho-pyridyl radical with 1,3-butadiene (right). Hatched areas indicate the acceptable upper and lower error limits of the fits. The solid red lines define the best-fit function.

both meta-pyridyl plus 1,3-butadiene and ortho-pyridyl plus 1,3-butadiene systems depict strong similarities. First, the translational energy distributions reveal maximum translational energy releases of  $124 \pm 20 \text{ kJ mol}^{-1}$  and  $122 \pm 42 \text{ kJ mol}^{-1}$ , respectively. By subtracting the collision energies of  $48.6 \pm 3.6 \text{ kJ mol}^{-1}$  and  $50.3 \pm 3.5 \text{ kJ mol}^{-1}$ , we obtain the reaction exoergicities of  $75 \pm 20 \text{ kJ mol}^{-1}$  and  $72 \pm 42 \text{ kJ mol}^{-1}$  in synthesizing  $C_9H_9N$  isomers plus atomic hydrogen. The larger uncertainty in the *o*-pyridyl–1,3-butadiene system is the result of the limited signal-to-noise of the reactive scattering signal obtained at  $m/z = 131$ . Second, CM translational energy distributions  $P(E_T)$  of the meta-pyridyl plus 1,3-butadiene and ortho-pyridyl plus 1,3-butadiene reactions exhibit distribution maxima at  $25\text{--}35 \text{ kJ mol}^{-1}$  and  $10\text{--}20 \text{ kJ mol}^{-1}$ , respectively. This “peaking away from zero translational energy” indicates

the existence of an exit barrier and a tight exit transition state to product formation (Levine 2005). On the other hand, peaking of the translational energy distribution close to zero translational energy would be indicative of a rather loose exit transition state and hence a simple bond rupture process.

The CM angular distributions ( $T(\theta)$ ) assist in collecting additional information on the reaction dynamics. In both systems, the  $T(\theta)$  present intensity over the whole angular range, indicating that the reactions follow indirect scattering dynamics through the formation of  $C_9H_{10}N$  intermediates with lifetimes longer than their rotational periods. Most importantly, for the meta-pyridyl–1,3-butadiene system, best fits were achieved with the  $T(\theta)$  depicting a pronounced distribution maximum at  $90^\circ$  with ratios of the flux intensities at the respective maxima and minima of the distribution,  $I(90^\circ)/I(0^\circ)$ ,

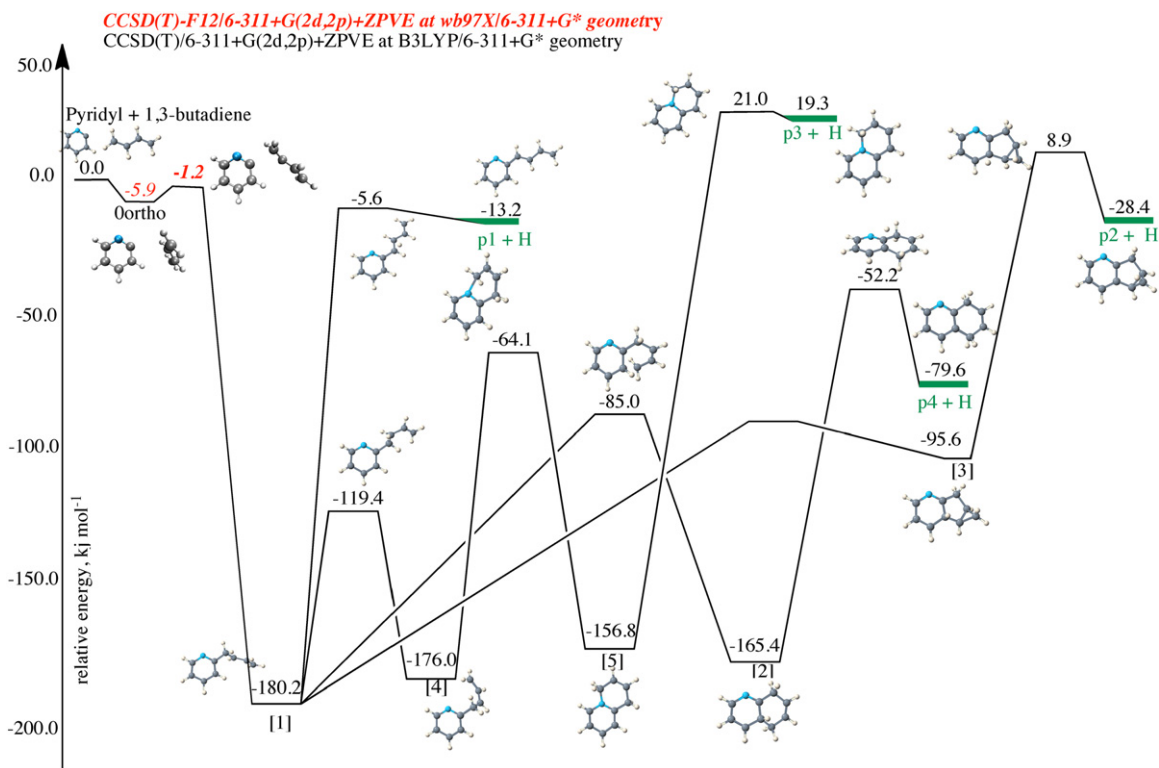


**Figure 4.** Potential energy diagram for the reaction of ortho-pyridyl plus 1,3-butadiene. Energies for intermediates, transition states, and products are given relative to the reactants (in  $\text{kJ mol}^{-1}$ ) at the CCSD(T)-F12/6-311+G(2d,2p)+ZPVE at  $\omega$ B97X/6-311+G\* optimized geometries for the sigma complex and associated TS, and CCSD(T)/6-311+G(2d,2p)+ZPVE at B3LYP/6-311+G\* optimized geometries for the rest.

of  $1.2 \pm 0.1$  to form  $\text{C}_9\text{H}_9\text{N}$  plus atomic hydrogen; this “sideways” scattering exposes the geometrical constraints of the fragmenting  $\text{C}_9\text{H}_{10}\text{N}$  intermediate(s) with the hydrogen atom being ejected almost parallel to the total angular momentum vector and hence perpendicular to the molecular plane of the rotating, decomposing complex(es).

### 4.3. Electronic Structure Calculations

The mechanisms and products formed in the reaction of pyridyl radicals (ortho-, meta-, and para- $\text{C}_5\text{H}_4\text{N}$ ;  $X^2A_1$ ) with 1,3-butadiene ( $X^1A'$ ) were investigated computationally by conducting ab initio calculations of the  $\text{C}_9\text{H}_{10}\text{N}$  PES. Addition can occur by any of the three pyridyl radical isomers (ortho-, meta-, and para- $\text{C}_5\text{H}_4\text{N}$ ;  $X^2A_1$ ) de-facto barrierlessly to the terminal  $\text{sp}^2$  hybridized carbon of the methylene moiety ( $\text{CH}_2$ ) of 1,3-butadiene (Figures 4–6). In addition to the terminal carbon atoms of 1,3-butadiene, the radical carbon atoms of *o*-, *m*-, and *p*-pyridyl and the terminal carbon atom of 1,3-butadiene follow an attractive minimum energy path under full geometry optimization, and form a van der Waals complex [ $0_{\text{ortho}}$ ,  $0_{\text{meta}}$ ,  $0_{\text{para}}$ ] with about a 3.3–3.5 Å equilibrium distance between the two carbon atoms with energies between 5 and 8  $\text{kJ mol}^{-1}$  below the separated reactants. A slight structural rearrangement of these van der Waals complexes over barriers of only 3–5  $\text{kJ mol}^{-1}$  leads to the initial intermediates [1], [6], and [11], respectively. The carbon–carbon distances reduce to about 2.5 Å in the transition states. The formation of these intermediates via van der Waals complexes and through barriers located below the energy of the reactants (submerged barriers) imply that these reactions are de-facto barrierless and can occur at very low temperatures, such as 10 K, prevailing in

cold molecular clouds. Previous studies of aromatic radicals (phenyl, tolyl) reacting with 1,3-butadiene have found the channel leading to addition of the radical carbon to the central carbon atom not to be competitive relative to the addition to the  $\text{CH}_2$  moiety even at elevated collision energies (Kaiser et al. 2012; Parker et al. 2014a; Muzangwa et al. 2015). The central addition channel pathways were, therefore, omitted from present consideration as a competing channel in low temperature interstellar environments. The structures of the exit transition states leading to the formation of 1,4-dihydroquinoline and 1,4-dihydroisoquinoline are presented in Figure 7, and the structures of the intermediates and products are presented in Figure 8.

The energies reported in the following sections were calculated using the CCSD(T) method along with the 6-311+G(2d,2p) basis set at the B3LYP/6-311+G\* optimized geometries. The transition states at the entrance channel are slightly below the dissociation limit. At the very low van der Waals binding energies of the weakly bound complexes, small corrections such as the basis set superposition error (BSSE), and zero point vibrational energy (ZPVE) become important. We calculated the binding energies of the transition states and sigma complexes using the explicitly correlated CCSD(T)-F12 method along with the same 6-311+G(2d,2p) basis set. The F12 methods essentially eliminate BSSE as has been demonstrated by Glob et al. (2012). Zero point vibrational energies calculated using the B3LYP ( $\omega$ B97X in the case of the weak interacting van der Waals complexes and TSs) were included in the single point CCSD(T) (or CCSD(T)-F12) energies. We checked the  $T_1$  diagnostics of all the calculated molecules and open shell radicals (Jayatilaka & Lee 1993). The  $T_1$  diagnostic values range from 0.017 to 0.021, which are within acceptable

values. While the B3LYP method reliably describes the geometries of the well-defined reactants and products, it has difficulty in predicting the geometries of the weakly interacting species, e.g., the van der Waals complexes and transition states of the entrance channel. B3LYP predicted binding distances that were too long (4.2 Å) for the van der Waals complexes due to its inherent deficiency in describing long-range interactions. The  $\omega$ B97X functional corrects for the long-range interaction and found the binding distances to be about 3.3–3.5 Å for the van der Waals complexes, and about 2.5 Å for the transition states at the entrance channel. The  $\omega$ B97X geometries for these species were used in the CCSD(T)-F12 calculations.

#### 4.3.1. Ortho-pyridyl Plus 1,3-butadiene

The addition of ortho-pyridyl to the terminal carbon of 1,3-butadiene leads to an initial van-der-Waals complex [ $0_{\text{ortho}}$ ]; the latter is bound by  $-5.9 \text{ kJ mol}^{-1}$  with respect to the separated reactants and isomerizes through a barrier of only  $4.7 \text{ kJ mol}^{-1}$  to the initial collision complex [1], which is stabilized by  $-180.2 \text{ kJ mol}^{-1}$  with respect to the separated reactants. [1] can eject a hydrogen atom to form trans-1-ortho-pyridyl-1,3-butadiene (p1) with an overall exoergicity of  $-13.2 \text{ kJ mol}^{-1}$ ; the associated exit transition state is located only  $7.6 \text{ kJ mol}^{-1}$  above the final products and hence is very loose. Alternately, cyclization of [1] can occur by the terminal  $\text{CH}_2$  group of the C4 chain binding to the adjacent carbon atom to form intermediate [3] stabilized by  $-95.6 \text{ kJ mol}^{-1}$ , though the associated transition state could not be located. Hydrogen emission from pyridyl ring  $\text{sp}^3$ -carbon yields an unusual tricyclic product p2 plus atomic hydrogen with an overall exoergicity of  $-28.4 \text{ kJ mol}^{-1}$  over a tight exit transition state located  $37.3 \text{ kJ mol}^{-1}$  above the separated products. However, a more energetically favorable channel for [1] is the rotation around a carbon-carbon single bond to [4] through a barrier of only  $60.8 \text{ kJ mol}^{-1}$  above [1]. Intermediate [4] can then cyclize forming [5] via a barrier of  $111.9 \text{ kJ mol}^{-1}$ . Intermediate [5] ejects a hydrogen atom through an exit transition state residing  $21 \text{ kJ mol}^{-1}$  above the separated reactants leading to the product p3 in an overall endoergic reaction of  $19.3 \text{ kJ mol}^{-1}$ . From intermediate [1], an alternative transition state exists, in which the C4 chain binds to the adjacent carbon atom to form [2]. Intermediate [2] is stabilized by  $-165.4 \text{ kJ mol}^{-1}$  with respect to the separated reactants, and can subsequently emit a hydrogen atom from the bridging carbon to yield the 1,4-dihydroquinoline product p4,  $-79.6 \text{ kJ mol}^{-1}$  below the reactants. To summarize, considering the transition states and required exoergicity of the overall reaction, the computations predict that the ortho pyridyl radical leads to intermediate [1] via a submerged barrier, which then isomerizes to [2] via a ring closure and terminates by atomic hydrogen loss and aromatization via a tight exit transition state to the 1,4-dihydroquinoline isomer p4.

#### 4.3.2. Meta-pyridyl Plus 1,3-butadiene

In analogy to the ortho-pyridyl radical, the addition of meta-pyridyl to the terminal carbon of 1,3-butadiene also forms a van-der-Waals complex [ $0_{\text{meta}}$ ] stabilized by  $8.4 \text{ kJ mol}^{-1}$  with respect to the separated reactants; the latter isomerizes through a barrier of  $4.5 \text{ kJ mol}^{-1}$  to the initial collision complex [6], which is stabilized by  $-166.9 \text{ kJ mol}^{-1}$ . Intermediate [6] can expel a hydrogen atom to form trans-1-meta-pyridyl-1,3-

butadiene (p5) with an overall exoergicity of  $29.7 \text{ kJ mol}^{-1}$  and a tight exit transition state of  $12.5 \text{ kJ mol}^{-1}$  above the products. Alternately, cyclization can occur by the terminal  $\text{CH}_2$  group of the C4 chain binding to the adjacent carbon atom to form a tricyclic intermediate [10] bound by  $-99.6 \text{ kJ mol}^{-1}$ . The transition state involving [6] and [10] could not be located. Hydrogen ejection yields product p6 with an overall exoergicity of  $45.6 \text{ kJ mol}^{-1}$  over a tight exit transition state located  $42.3 \text{ kJ mol}^{-1}$  above the separated products. Also, intermediate [6] was predicted to isomerize via ring closures to intermediate [9] and—after rotation around the carbon-carbon single bond via intermediate [7] eventually to intermediate [8]. Intermediates [7], [8], and [9] are stabilized by  $-191.7$ ,  $-185.8$ , and  $-176.2 \text{ kJ mol}^{-1}$  with respect to the separated reactants and can decompose via atomic hydrogen loss leading to 1,4-dihydroquinoline (p4) and 1,4-dihydroisoquinoline (p7) in overall exoergic reactions ( $-102.1$  and  $-97.1 \text{ kJ mol}^{-1}$ ), respectively. Based on the energies of the transition states, the meta-pyridyl radical, via a submerged barrier, forms intermediate [6], which isomerizes via ring closure to intermediates [8] and [9]. A terminal atomic hydrogen loss accompanied by aromatization via tight exit transition states is expected to form 1,4-dihydroquinoline (p4) and a minor amount of 1,4-dihydroisoquinoline (p7).

#### 4.3.3. Para-pyridyl Plus 1,3-butadiene

The addition of para-pyridyl to the terminal carbon of 1,3-butadiene is also barrierless leading via a van-der-Waals complex [ $0_{\text{para}}$ ] and a submerged barrier located  $1.8 \text{ kJ mol}^{-1}$  below the energy of the separated reactants to intermediate [11], which is stabilized by  $-187.7 \text{ kJ mol}^{-1}$  with respect to the separated reactants. The latter can react via three pathways. First, intermediate [11] can expel a hydrogen atom to form trans-1-para-pyridyl-1,3-butadiene (p8) with an overall exoergicity of  $-26.7 \text{ kJ mol}^{-1}$  and a tight exit transition state of  $12.4 \text{ kJ mol}^{-1}$ . Alternately, cyclization can occur forming the tricyclic intermediate [14] and—via rotation around the carbon-carbon single bond via intermediate [12]—to intermediate [13]. The transition states involving all of the steps were located, except for the one involving [11] and [14]. Hydrogen ejection from bridging pyridyl ring  $\text{sp}^3$ -carbon yields product p6 with an exoergicity of  $-43.5 \text{ kJ mol}^{-1}$  over a tight exit transition state. The most energetically favorable pathway involves intermediate [13] emitting a hydrogen atom. This process forms the aromatic 1,4-dihydroisoquinoline (p7) product in an overall exoergic reaction ( $-92.3 \text{ kJ mol}^{-1}$ ) through a tight exit transition state located  $73.4 \text{ kJ mol}^{-1}$  above the separated products.

## 5. REACTION MECHANISM

We are now merging the computational results with the experimental data in an attempt to elucidate the underlying reaction pathway(s). First, let us inspect the reaction products most likely formed in the meta-pyridyl—1,3-butadiene system. Here, the experimentally determined reaction energy of  $75 \pm 20 \text{ kJ mol}^{-1}$  correlates well with the calculations for the formation of the 1,4-dihydroquinoline isomer (p4) and/or the 1,4-dihydroisoquinoline structure (p7). The formation of these isomers proceeds via intermediates [8] and [9] through tight transition states located  $27.9$  and  $41.4 \text{ kJ mol}^{-1}$  above the separated products. Recall that the nature of a tight exit

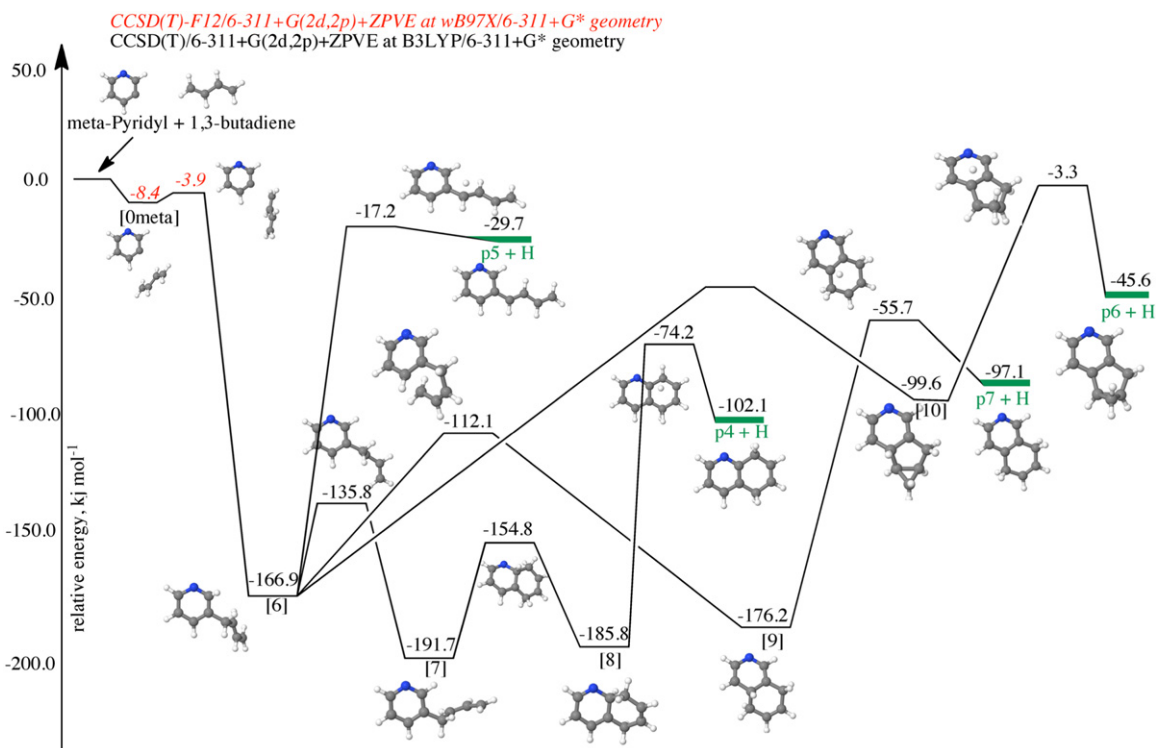


**Figure 5.** Potential energy diagram for the reaction of meta-pyridyl plus 1,3-butadiene. Energies for intermediates, transition states, and products are given relative to the reactants (in  $\text{kJ mol}^{-1}$ ) at the CCSD(T)-F12/6-311+G(2d,2p)+ZPVE at  $\omega\text{B97X}/6\text{-}311+\text{G}^*$  optimized geometries for sigma complex and associated TS, and CCSD(T)/6-311+G(2d,2p)+ZPVE at B3LYP/6-311+G\* optimized geometries for the rest.

transition state was predicted based on the off-zero peaking of the CM translational energy distribution. A close look at the geometries of these exit transition states suggests that the hydrogen atom is emitted at  $92.5^\circ$  and  $93.1^\circ$  with respect to the rotational plane of the decomposing complex (Figure 7). Therefore, both exit transition states could explain the experimental findings of a “sideways scattering,” i.e., an elimination of the hydrogen atom almost parallel to the total angular momentum vector. On the molecular level, the reversed reaction, i.e., the addition of a hydrogen atom to the aromatic  $\pi$ -system, would proceed perpendicularly to the molecular plane as dictated by the geometry of the orbitals.

Second, we analyze the reaction products most likely synthesized in the reaction of the ortho-pyridyl radical with 1,3-butadiene. Our experimentally determined reaction energy of  $72 \pm 42 \text{ kJ mol}^{-1}$  matches best the computed data leading to the formation of 1,4-dihydroquinoline (p4) plus atomic hydrogen ( $-79.6 \text{ kJ mol}^{-1}$ ). This isomer is accessed from intermediate [2] by passing through a tight transition state placed  $27.4 \text{ kJ mol}^{-1}$  above the energy of the separated products. The tight nature of this exit transition state was predicted based on the off-zero peaking of the CM translational energy distribution at  $10\text{--}20 \text{ kJ mol}^{-1}$ . Considering the limited reactive scattering signal and the resulting error limits of the CM functions, it is difficult to analyze the geometries of these exit transition states and to compare the hydrogen loss geometry with the experimental findings. For completeness, the calculations predict that the hydrogen atom is lost at  $93.6^\circ$  with respect to the rotational plane of the decomposing complex. Experimentally, it was observed that the meta isomer is more reactive compared to the ortho isomer. Our ab initio calculations suggest (Figures 5 and 6) that the van der Waal’s

complex associated with the ortho isomer sees a slightly larger barrier compared to the meta isomer in the entrance channel, which is the slowest step in the reaction sequence. Additionally, the van der Waal’s complex of meta-pyridyl is more tightly bound compared to the van der Waal’s complex of ortho-pyridyl with butadiene.

Based on these considerations, we propose the following reaction mechanisms; for completeness, we also integrate our computational findings for the para-pyridyl radical. The reactions of the ortho-, meta-, and para-pyridyl radicals undergo similar chemical dynamics and are initiated by the formation of a van-der-Waals complexes  $[\text{o}_{\text{ortho}}]$ ,  $[\text{o}_{\text{meta}}]$ , and  $[\text{o}_{\text{para}}]$ , which are weakly bound by  $5.1\text{--}8.4 \text{ kJ mol}^{-1}$  with respect to the separated reactants. These complexes isomerize via addition to the radical center to the terminal C1 carbon atoms of 1,3-butadiene via small barriers of only  $3.3\text{--}4.7 \text{ kJ mol}^{-1}$  forming RSFR intermediates [1], [6], and [11] bound by  $180.2$ ,  $166.9$ , and  $187.7 \text{ kJ mol}^{-1}$ , respectively. At low temperature ( $\sim 10 \text{ K}$ ) the entropy change associated with the cyclization plays a very small role, and the enthalpy-difference largely outweighs the energy contribution from entropy loss due to cyclization. In all cases, the barrier to addition lies below the energy of the separated reactants (submerged barrier). This holds strong implications for the chemistry in cold molecular clouds because these reactions are de-facto barrier-less and hence can happen in cold molecular clouds such as TMC-1 and OMC-1. The RSFR intermediates eventually undergo cyclization to [2], [8]/[9], and [13] before they undergo unimolecular decomposition via atomic hydrogen loss and hence the formation of aromatic products 1,4-dihydroquinoline isomer (p4) [o-pyridyl], 1,4-dihydroquinoline (p4) and/or 1,4-dihydroisoquinoline (p7) [m-pyridyl], and 1,4-

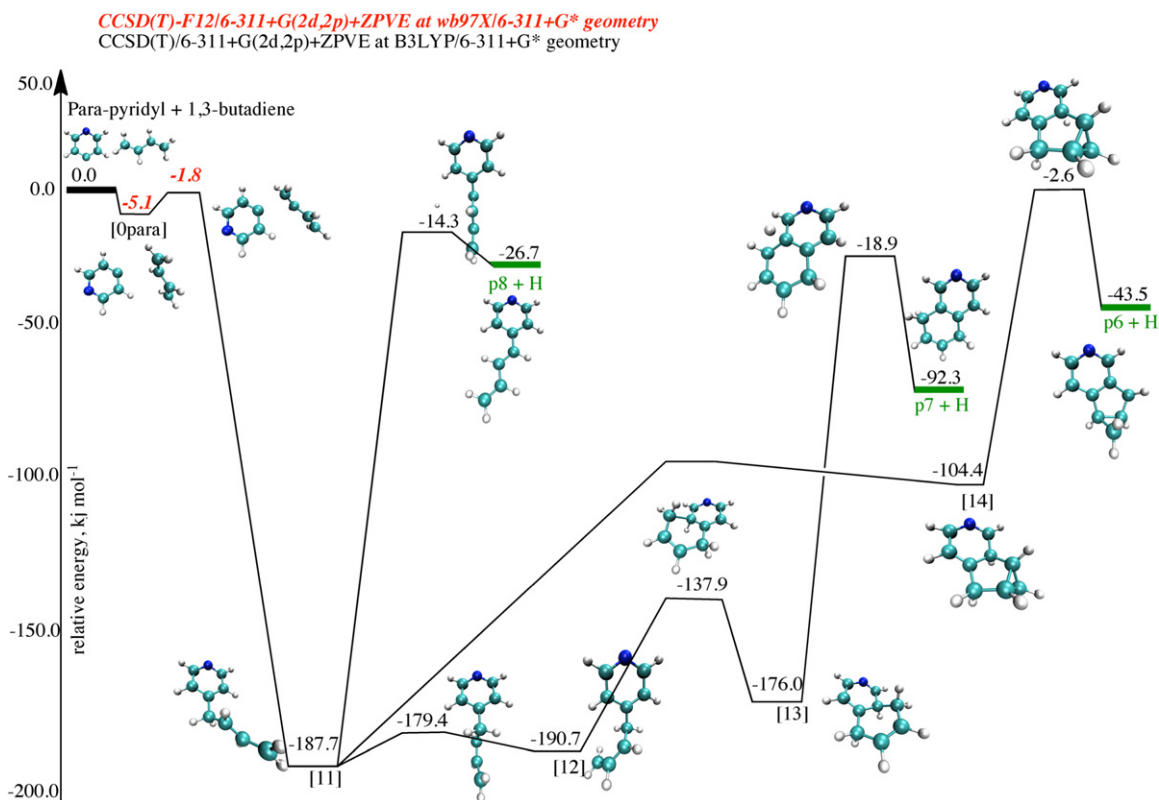


**Figure 6.** Potential energy diagram for the reaction of para-pyridyl plus 1,3-butadiene. Energies for intermediates, transition states, and products are given relative to the reactants (in  $\text{kJ mol}^{-1}$ ) at the CCSD(T)-F12/6-311+G(2d,2p)+ZPVE at  $\omega$ B97X/6-311+G\* optimized geometries for the sigma complex and associated TS, and CCSD(T)/6-311+G(2d,2p)+ZPVE at B3LYP/6-311+G\* optimized geometries for the rest.

dihydroisoquinoline (p7). In all cases, the hydrogen atom is emitted almost perpendicularly to the molecular plane of the decomposing complex from the bridging carbon atom. It is important to highlight that the nitrogen atom is always located in p4 and p7 in the “outer” ring; formation of products (p3) with the nitrogen atom bridging both six-membered rings was found to be energetically not competitive.

This mechanism adds to the increasing catalog of reactions involving phenyl-type aromatic radicals with the radical located on the aromatic ring, such as phenyl (Kaiser et al. 2012), para-tolyl (Parker et al. 2014a), and meta-tolyl (Muzangwa et al. 2015) with 1,3-butadiene and vinylacetylene that lead to facile PAH formation at low temperatures, through the formation of a van der Waals complex. PANH formation at low temperatures has implications for the astrochemistry of biologically relevant molecules. It should be noted that under our experimental conditions monocyclic products such as p1, p5, and p8 could be produced by overcoming a higher entrance barrier. However, the existence of an entrance barrier implies that the reaction channels are closed in cold environments such as in cold molecular clouds where average temperatures of 10 K reside.

Finally, we would like to compare our experimental findings and conclusions with predictions based on statistical (RRKM) calculations conducted for a range of collision energies from 0 to  $30 \text{ kJ mol}^{-1}$  in increments of  $10 \text{ kJ mol}^{-1}$ . The RRKM product branching ratios are reported in Table 2. The forward and reverse RRKM rate constants of all individual reaction steps of the ortho-, meta-, and para-pyridyl radical addition to the terminal  $\text{CH}_2$   $\text{sp}^2$ -carbon of 1,3-butadiene are given in Tables 3–5. The RRKM branching ratios indicate that for the

reaction between ortho-pyridyl radical and 1,3-butadiene, 1,4-dihydroquinoline (p4) plus a hydrogen atom are the major products at collision energies from 0 to  $30 \text{ kJ mol}^{-1}$ . This can be rationalized easily since p4 forms through the lowest energy transition state(s) as seen in Figure 4 essentially favoring the reaction sequence [1]  $\rightarrow$  [2]  $\rightarrow$  p4 + H. The branching ratios calculated for the meta-pyridyl plus 1,3-butadiene reaction (Figure 5) once again predict that p4, i.e., 1,4-dihydroquinoline, represents the major product under single collision conditions with collision energies ranging from 0 to  $30 \text{ kJ mol}^{-1}$ . This can be rationalized considering the low energy transition states in the reaction sequence [6]  $\rightarrow$  [7]  $\rightarrow$  [8]  $\rightarrow$  p4 + H, which is favorable compared to the [6]  $\rightarrow$  [9]  $\rightarrow$  p7 + H mechanism. The branching ratios for the reaction of 1,3-butadiene with a para-pyridyl radical are rather interesting as the alternative isomer p7 has a significant predicted abundance at zero collision energy. The predicted branching ratio depends on the collision energy with an enhanced collision energy leading to a decrease of p7. This is probably the case because the two competing mechanisms from [11] in this case have similar exit transition state energies (Figure 6).

## 6. ASTROPHYSICAL IMPLICATIONS AND CONCLUSIONS

The *barrierless* formation of 1,4-dihydroquinoline and 1,4-dihydroisoquinoline ( $\text{C}_9\text{H}_9\text{N}$ ) provides compelling evidence that PANHs and their partially hydrogenated counterparts can be synthesized in the gas phase at ultra-low temperatures of cold molecular clouds even down to 10 K via the reaction of the

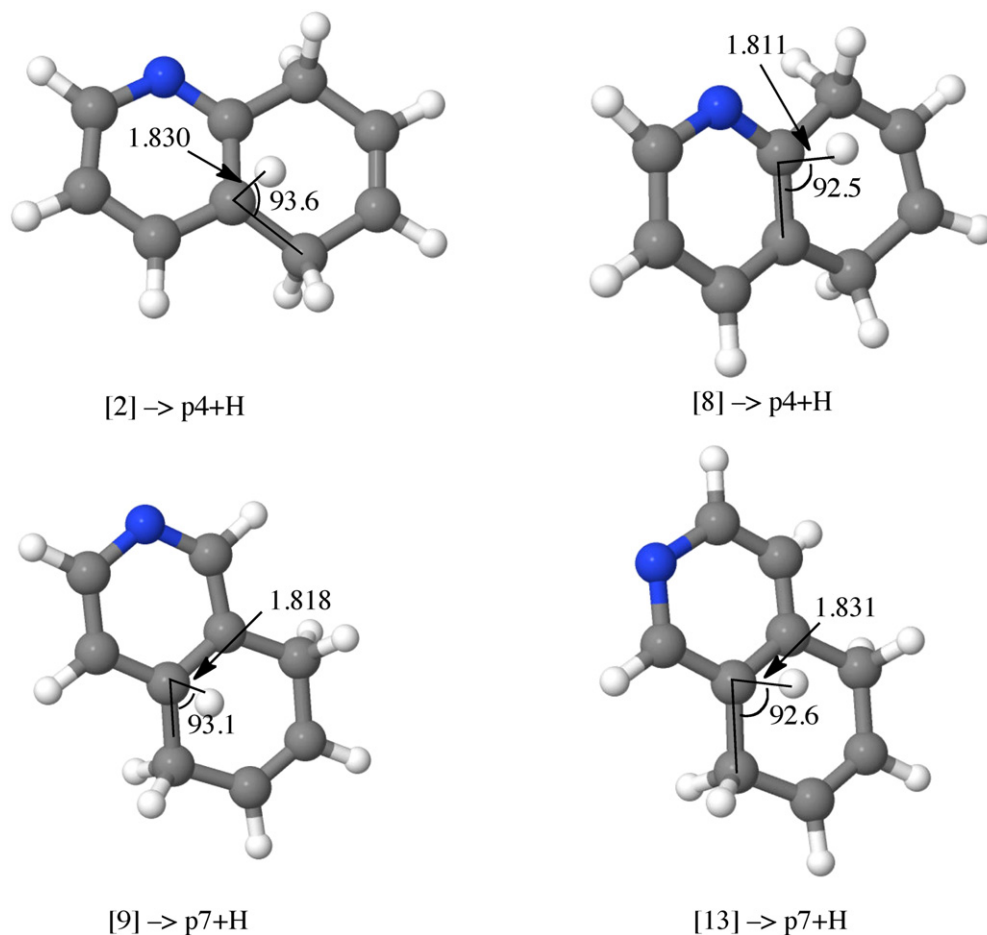


**Figure 7.** Structures of the exit transition states leading to the formation of 1,4-dihydroquinoline (p4) and 1,4-dihydroisoquinoline (p7) isomers.

**Table 2**

Calculated Product Branching Ratios of the Reactions of 1,3-butadiene with Ortho-, Meta-, and Para-pyridyl Radicals at Different Collision Energies under Single Collision Conditions

Reactants and products	Collision Energy (kJ mol <sup>-1</sup> )			
	0	10	20	30
Ortho-pyridyl + 1,3 butadiene (Figure 4)				
p1 + H	0	0	0	0
p3 + H	0	0	0	0
p4 + H	100	100	100	100
Meta-pyridyl + 1,3 butadiene (Figure 5)				
p4 + H	100	100	100	100
p5 + H	0	0	0	0
p7 + H	0	0	0	0
Para-pyridyl + 1,3 butadiene (Figure 6)				
p7 + H	18	13	8	6
p8 + H	82	87	92	94

meta-pyridyl, ortho-pyridyl, and para-pyridyl radicals with the 1,3-butadiene molecule via a single collision event. It is important to reiterate that as the pyridyl radical (ortho, meta, and para) approaches 1,3-butadiene, long range attractive van der Waals forces cause the entrance barrier for addition to be circumnavigated without any energy required, i.e., no translational energy. Therefore, at very low temperatures of cold molecular clouds, such as in TMC-1 with average temperatures

of about 10 K, the reaction will still be able to proceed. These reactions form part of a growing group of de facto barrierless-type reactions, leading to aromatization to PAH-type species at ultralow temperatures, involving aromatic radicals with the radical located on the aromatic ring that undergo addition to a C4 double conjugated unsaturated hydrocarbon such as 1,3-butadiene (C<sub>4</sub>H<sub>6</sub>) or vinylacetylene (C<sub>4</sub>H<sub>4</sub>; Kaiser et al. 2012; Parker et al. 2012a, 2014a, 2014b, 2015; Dangi et al. 2014; Kaiser et al. 2015; Muzangwa et al. 2015; Yang et al. 2015). Previously, aromatization reactions had been calculated to proceed over an energy barrier implying that they could only be formed in high temperature environments such as in the inner regions of circumstellar envelopes of dying carbon stars like IRC+10216 to supply the necessary kinetic transitional energy to overcome the barriers (Tielens et al. 2000; Kislov et al. 2005; Tielens 2008; Cherchneff 2011). Although, circumstellar envelopes are highly relevant to organic radical mediated astrochemistry, the discovery of ultra-low temperature reaction channels of aromatization-type reactions leading to PAHs and their nitrogen substituted counterparts implies that they could operate at much greater proportions not restricted to only high temperature environments. Considering nitrogen is isoelectronic with the CH moiety in an aromatic system, organic aromatics containing nitrogen atoms could follow similar mechanisms. We anticipate that pyridyl radicals could be present considering the large array of nitriles such as vinylcyanide (C<sub>2</sub>H<sub>3</sub>CN) (Gardner & Winnewisser 1975) and cyanoacetylene (HCCCN; Turner 1971) detected in the ISM. Benzene has been shown to

**Table 3**  
Individual Rate Constants of the Forward and Backward Reactions  
of Ortho-pyridyl with 1,3-butadiene

Energy		0.00	TS	$k$ ( $s^{-1}$ )	$k(\text{tun}) s^{-1}$
[1]	$\Rightarrow$	[4]	1	1.44E+11	1.45E+11
[4]	$\Rightarrow$	[1]	1	4.92E+09	4.95E+09
[1]	$\Rightarrow$	[2]	3	6.07E+06	6.44E+06
[2]	$\Rightarrow$	[1]	3	9.83E+07	1.04E+08
[1]	$\Rightarrow$	p1	4	2.40E-02	3.58E-02
[1]	$\Rightarrow$	[0ortho]	7	1.43E-03	1.93E-03
[0ortho]	$\Rightarrow$	[1]	7	1.74E+09	2.35E+09
[4]	$\Rightarrow$	[5]	2	6.10E+03	6.58E+03
[5]	$\Rightarrow$	[4]	2	5.55E+06	5.98E+06
[5]	$\Rightarrow$	p3	5	0.00E+00	4.55E-94
[2]	$\Rightarrow$	p4	6	2.20E+05	2.64E+05
Energy		2.39			
[1]	$\Rightarrow$	[4]	1	2.00E+11	2.01E+11
[4]	$\Rightarrow$	[1]	1	6.57E+09	6.61E+09
[1]	$\Rightarrow$	[2]	3	1.07E+07	1.13E+07
[2]	$\Rightarrow$	[1]	3	1.64E+08	1.73E+08
[1]	$\Rightarrow$	p1	4	1.19E+00	1.41E+00
[1]	$\Rightarrow$	[0ortho]	7	3.78E-01	3.98E-01
[0ortho]	$\Rightarrow$	[1]	7	7.15E+09	7.52E+09
[4]	$\Rightarrow$	[5]	2	1.31E+04	1.40E+04
[5]	$\Rightarrow$	[4]	2	1.13E+07	1.21E+07
[5]	$\Rightarrow$	p3	5	0.00E+00	5.46E-94
[2]	$\Rightarrow$	p4	6	5.60E+05	6.54E+05
Energy		4.78			
[1]	$\Rightarrow$	[4]	1	2.72E+11	2.73E+11
[4]	$\Rightarrow$	[1]	1	8.56E+09	8.60E+09
[1]	$\Rightarrow$	[2]	3	1.79E+07	1.88E+07
[2]	$\Rightarrow$	[1]	3	2.59E+08	2.72E+08
[1]	$\Rightarrow$	p1	4	1.54E+01	1.72E+01
[1]	$\Rightarrow$	[0ortho]	7	5.97E+00	6.13E+00
[0ortho]	$\Rightarrow$	[1]	7	8.61E+09	8.85E+09
[4]	$\Rightarrow$	[5]	2	2.58E+04	2.74E+04
[5]	$\Rightarrow$	[4]	2	2.12E+07	2.25E+07
[5]	$\Rightarrow$	p3	5	0.00E+00	6.52E-94
[2]	$\Rightarrow$	p4	6	1.27E+06	1.46E+06
Energy		7.17			
[1]	$\Rightarrow$	[4]	1	3.60E+11	3.62E+11
[4]	$\Rightarrow$	[1]	1	1.09E+10	1.09E+10
[1]	$\Rightarrow$	[2]	3	2.86E+07	2.99E+07
[2]	$\Rightarrow$	[1]	3	3.93E+08	4.11E+08
[1]	$\Rightarrow$	p1	4	1.12E+02	1.21E+02
[1]	$\Rightarrow$	[0ortho]	7	4.54E+01	4.62E+01
[0ortho]	$\Rightarrow$	[1]	7	9.27E+09	9.44E+09
[4]	$\Rightarrow$	[5]	2	4.74E+04	4.99E+04
[5]	$\Rightarrow$	[4]	2	3.73E+07	3.92E+07
[5]	$\Rightarrow$	p3	5	2.69E-02	2.74E-02
[2]	$\Rightarrow$	p4	6	2.64E+06	2.97E+06

be formed in the ISM by reactions of ethynyl radicals with 1,3-butadiene (Jones et al. 2011) and aromatic radical phenyl ( $C_6H_5$ ) can be synthesized in circumstellar shells (Frenklach & Feigelson 1989). Small hydrocarbons such as 1,3-butadiene can be formed in circumstellar envelopes of carbon stars through the reaction of methylidyne (CH) first with ethane ( $C_2H_6$ ) to form propene ( $C_3H_6$ ) plus hydrogen, then methylidyne (CH) could react with propene ( $C_3H_6$ ) to form 1,3-butadiene ( $C_4H_6$ ); Jones et al. 2011).

Following the expected presence of PANHs in the ISM, astronomical searches for pyridine, pyrimidine, quinoline, and isoquinoline were conducted (Kuan et al. 2003; Charnley et al. 2005); however, no positive assignments were made. The

**Table 4**  
Individual Rate Constants of the Forward and Backward Reactions  
of Meta-pyridyl with 1,3-butadiene

Energy		0.00	TS	$k$ ( $s^{-1}$ )	$k(\text{tun}) s^{-1}$
[0meta]	$\Rightarrow$	[6]	1	2.02E+10	2.06E+10
[6]	$\Rightarrow$	[0meta]	1	4.87E-02	4.96E-02
[6]	$\Rightarrow$	[7]	2	1.25E+12	1.26E+12
[7]	$\Rightarrow$	[6]	2	1.13E+11	1.14E+11
[6]	$\Rightarrow$	[9]	7	9.03E+07	9.41E+07
[9]	$\Rightarrow$	[6]	7	2.94E+09	3.06E+09
[6]	$\Rightarrow$	p5	6	1.62E+00	1.98E+00
[7]	$\Rightarrow$	[8]	3	1.18E+09	1.19E+09
[8]	$\Rightarrow$	[7]	3	1.19E+11	1.19E+11
[8]	$\Rightarrow$	p4	4	1.61E+08	1.75E+08
[9]	$\Rightarrow$	p7	5	1.95E+05	2.38E+05
Energy		2.39			
[0meta]	$\Rightarrow$	[6]	1	8.38E+10	8.45E+10
[6]	$\Rightarrow$	[0meta]	1	7.64E+00	7.70E+00
[6]	$\Rightarrow$	[7]	2	1.46E+12	1.47E+12
[7]	$\Rightarrow$	[6]	2	1.45E+11	1.45E+11
[6]	$\Rightarrow$	[9]	7	1.19E+08	1.23E+08
[9]	$\Rightarrow$	[6]	7	4.11E+09	4.27E+09
[6]	$\Rightarrow$	p5	6	1.64E+01	1.87E+01
[7]	$\Rightarrow$	[8]	3	1.33E+09	1.33E+09
[8]	$\Rightarrow$	[7]	3	1.34E+11	1.34E+11
[8]	$\Rightarrow$	p4	4	3.43E+08	3.69E+08
[9]	$\Rightarrow$	p7	5	4.90E+05	5.81E+05
Energy		4.78			
[0meta]	$\Rightarrow$	[6]	1	1.23E+11	1.24E+11
[6]	$\Rightarrow$	[0meta]	1	1.18E+02	1.19E+02
[6]	$\Rightarrow$	[7]	2	1.69E+12	1.70E+12
[7]	$\Rightarrow$	[6]	2	1.82E+11	1.83E+11
[6]	$\Rightarrow$	[9]	7	1.52E+08	1.57E+08
[9]	$\Rightarrow$	[6]	7	5.60E+09	5.79E+09
[6]	$\Rightarrow$	p5	6	9.89E+01	1.09E+02
[7]	$\Rightarrow$	[8]	3	1.47E+09	1.48E+09
[8]	$\Rightarrow$	[7]	3	1.49E+11	1.49E+11
[8]	$\Rightarrow$	p4	4	6.78E+08	7.23E+08
[9]	$\Rightarrow$	p7	5	1.11E+06	1.28E+06
Energy		7.17			
[0meta]	$\Rightarrow$	[6]	1	1.51E+11	1.52E+11
[6]	$\Rightarrow$	[0meta]	1	8.84E+02	8.87E+02
[6]	$\Rightarrow$	[7]	2	1.94E+12	1.95E+12
[7]	$\Rightarrow$	[6]	2	2.26E+11	2.27E+11
[6]	$\Rightarrow$	[9]	7	1.91E+08	1.97E+08
[9]	$\Rightarrow$	[6]	7	7.42E+09	7.67E+09
[6]	$\Rightarrow$	p5	6	4.34E+02	4.69E+02
[7]	$\Rightarrow$	[8]	3	1.63E+09	1.63E+09
[8]	$\Rightarrow$	[7]	3	1.65E+11	1.65E+11
[8]	$\Rightarrow$	p4	4	1.26E+09	1.33E+09
[9]	$\Rightarrow$	p7	5	2.29E+06	2.60E+06

upper limit on the column density for pyridine and quinoline in the post-AGB object GL 618 is about  $3 \times 10^{13} \text{ cm}^{-2}$  for an adopted temperature of 200 K. Furthermore, PANHs might be subject to photo destruction by ultraviolet radiation, which was recently demonstrated experimentally (Peeters et al. 2005). Nevertheless, PANHs such as quinoline have been found in large proportions in the Murchison and Lonewolf Nunataks 94102 meteorites (Stoks & Schwartz 1982). Here, neutral-neutral gas phase reactions can provide a mechanism by which acyclic and monocyclic organic species containing nitrogen atoms can form PANHs. These PANHs could be further condensed onto icy mantles of interstellar dust grains, where they can become the molecular backbone onto which

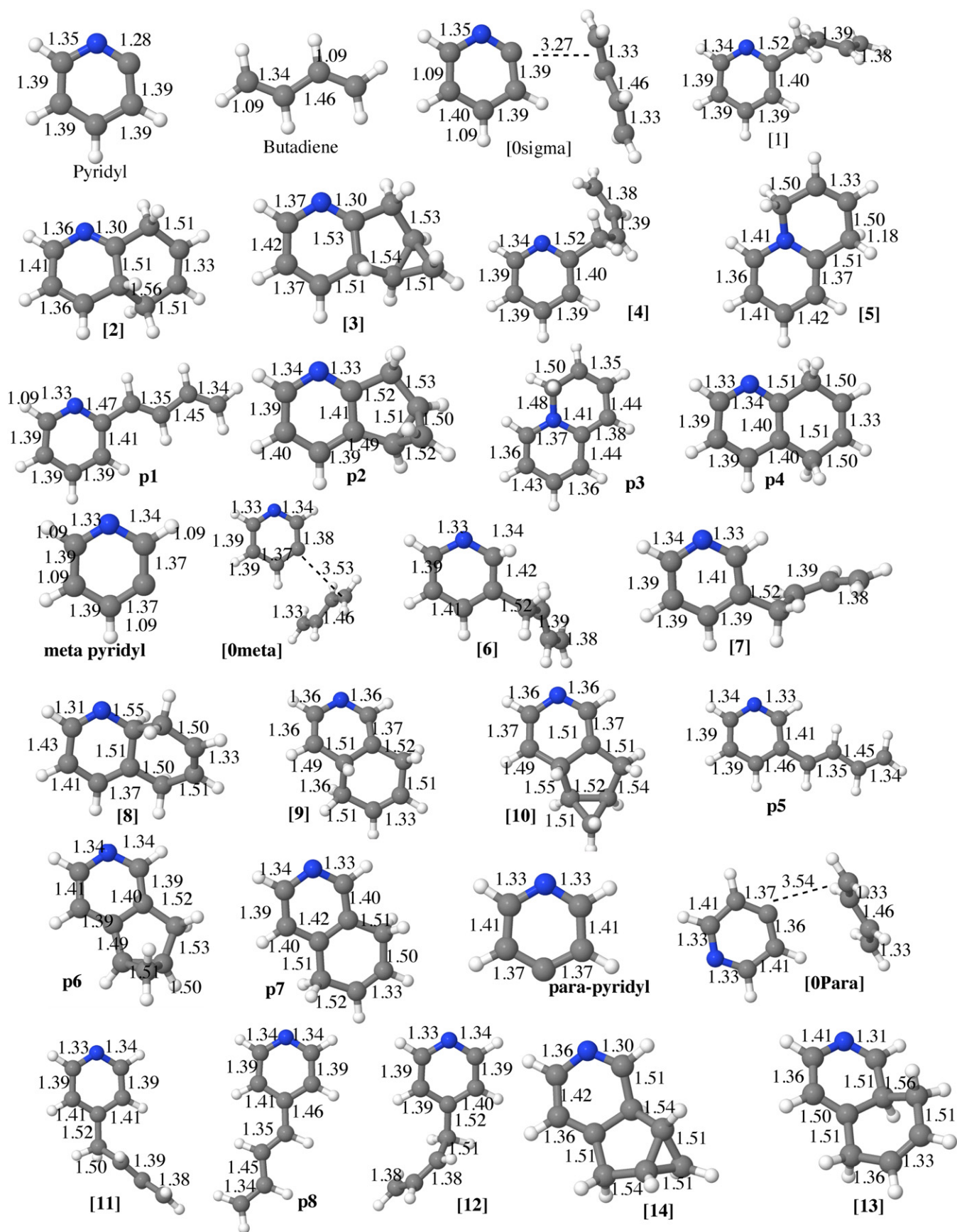


**Figure 8.** Structures of reactants, intermediates, and products in the reactions of ortho-, meta-, and para-pyridyl radicals with 1,3-butadiene. Bond lengths are given in Angstrom.

**Table 5**  
Individual Rate Constants of the Forward and Backward Reactions  
of Para-pyridyl with 1,3-butadiene

Energy	is:	0.00	TS	$k$ ( $s^{-1}$ )	$k(\text{tun}) s^{-1}$
Opara	$\Rightarrow$	[11]	1	2.21E+10	2.71E+10
[11]	$\Rightarrow$	Opara	1	1.08E-04	1.33E-04
[11]	$\Rightarrow$	[12]	2	5.40E+11	5.41E+11
[12]	$\Rightarrow$	[11]	2	2.15E+12	2.15E+12
[11]	$\Rightarrow$	p8	5	2.72E-02	3.32E-02
[12]	$\Rightarrow$	[13]	3	2.39E+08	2.39E+08
[13]	$\Rightarrow$	[12]	3	2.24E+10	2.24E+10
[13]	$\Rightarrow$	p7	4	2.66E+00	4.33E+00
Energy		2.39 $\text{kJ mol}^{-1}$			
Opara	$\Rightarrow$	[11]	1	1.19E+11	1.22E+11
[11]	$\Rightarrow$	Opara	1	5.33E-02	5.48E-02
[11]	$\Rightarrow$	[12]	2	5.57E+11	5.57E+11
[12]	$\Rightarrow$	[11]	2	2.24E+12	2.24E+12
[11]	$\Rightarrow$	p8	5	3.75E-01	4.25E-01
[12]	$\Rightarrow$	[13]	3	2.90E+08	2.90E+08
[13]	$\Rightarrow$	[12]	3	2.63E+10	2.64E+10
[13]	$\Rightarrow$	p7	4	1.69E+01	2.42E+01
Energy		4.78			
Opara	$\Rightarrow$	[11]	1	1.59E+11	1.61E+11
[11]	$\Rightarrow$	Opara	1	1.05E+00	1.06E+00
[11]	$\Rightarrow$	[12]	2	5.73E+11	5.73E+11
[12]	$\Rightarrow$	[11]	2	2.33E+12	2.33E+12
[11]	$\Rightarrow$	p8	5	2.77E+00	3.03E+00
[12]	$\Rightarrow$	[13]	3	3.45E+08	3.46E+08
[13]	$\Rightarrow$	[12]	3	3.06E+10	3.06E+10
[13]	$\Rightarrow$	p7	4	7.57E+01	1.01E+02
Energy		7.17			
Opara	$\Rightarrow$	[11]	1	1.81E+11	1.83E+11
[11]	$\Rightarrow$	Opara	1	9.03E+00	9.12E+00
[11]	$\Rightarrow$	[12]	2	5.88E+11	5.89E+11
[12]	$\Rightarrow$	[11]	2	2.42E+12	2.41E+12
[11]	$\Rightarrow$	p8	5	1.42E+01	1.52E+01
[12]	$\Rightarrow$	[13]	3	4.07E+08	4.07E+08
[13]	$\Rightarrow$	[12]	3	3.51E+10	3.51E+10
[13]	$\Rightarrow$	p7	4	2.70E+02	3.42E+02

substitution reactions can form nucleobase-type structures such as purines via non-equilibrium chemistry (Maity et al. 2014).

The experimental work was supported by the Department of Energy, Basic Energy Sciences (DE-FG02-03ER15411) at the University of Hawaii (R.I.K.). This research was also supported by a Postdoctoral Fellow Appointment by the NASA Postdoctoral Program (D.S.N.P.) administered by Oak Ridge Associated Universities through a contract with NASA. The computations are based upon work supported by the National Aeronautics and Space Administration through the NASA Astrobiology Institute under Cooperative Agreement Notice NNH13ZDA017C issued through the Science Mission Directorate. Computational work was performed using the Pleiades supercomputer of the NASA Advanced Supercomputing Division, and our in-house computers. The authors would like to thank Prof. Alexander Mebel for sharing his RRKM code.

## REFERENCES

- Balucani, N., Asvany, O., Kaiser, R. I., & Osamura, Y. 2002, *JPCA*, **106**, 4301  
Balucani, N., Mebel, A. M., Lee, Y. T., & Kaiser, R. I. 2001, *JPCA*, **105**, 9813  
Becke, A. D. 1993, *JCP*, **98**, 5648  
Bernstein, M. P., Sandford, S. A., Allamandola, L. J., et al. 1999, *Sci*, **283**, 1135  
Callahan, M. P., Smith, K. E., Cleaves, H. J., II, et al. 2011, *PNAS*, **108**, 13995  
Chai, J.-D., & Head-Gordon, M. 2008, *JCP*, **128**, 084106  
Charnley, S. B., Kuan, Y. J., Huang, H. C., et al. 2005, *AdSpR*, **36**, 137  
Cherchneff, I. 2011, *EASPS*, **46**, 177  
Clark, T., Chandrasekhar, J., Spitznagel, G. W., & Schleyer, P. v. R. 1983, *JCC*, **4**, 294  
Dangi, B. B., Yang, T., Kaiser, R. I., & Mebel, A. M. 2014, *PCCP*, **16**, 16805  
Ehrenfreund, P., & Sephton, M. A. 2006, *FaDi*, **133**, 277  
Frenklach, M., & Feigelson, E. D. 1989, *ApJ*, **341**, 372  
Frisch, M. J., Pople, J. A., & Binkley, J. S. 1984, *JCP*, **80**, 3265  
Gardner, F. F., & Winnewisser, G. 1975, *ApJL*, **195**, L127  
Glob, A., Brandle, M. P., Klopfer, W., & Luthi, H. P. 2012, *MolPh*, **110**, 2523  
Golan, A., Ahmed, M., Mebel, A. M., & Kaiser, R. I. 2013, *PCCP*, **15**, 341  
Hamid, A. M., Bera, P. P., Lee, T. J., et al. 2014a, *JPCL*, **5**, 3392  
Hamid, A. M., El-Shall, M. S., Hilal, R., Elroby, S., & Aziz, S. G. 2014b, *JCP*, **141**, 054305  
Herbst, E., & van Dishoeck, E. F. 2009, *ARA&A*, **47**, 427  
Hudgins, D. M., Bauschlicher, C. W., Jr., & Allamandola, L. J. 2005, *ApJ*, **632**, 316  
Jayatilaka, D., & Lee, T. J. 1993, *JCP*, **98**, 9734  
Jones, B. M., Zhang, F., Kaiser, R. I., et al. 2011, *PNAS*, **108**, 452  
Kaiser, R. I., Balucani, N., Charkin, D. O., & Mebel, A. M. 2003, *CPL*, **382**, 112  
Kaiser, R. I., Chiong, C. C., Asvany, O., et al. 2001, *JCP*, **114**, 3488  
Kaiser, R. I., Hahndorf, I., Huang, L. C. L., et al. 1999a, *JCP*, **110**, 6091  
Kaiser, R. I., Maksyutenko, P., Ennis, C., et al. 2010, *FaDi*, **147**, 429  
Kaiser, R. I., Mebel, A. M., Chang, A. H. H., Lin, S. H., & Lee, Y. T. 1999b, *JCP*, **110**, 10330  
Kaiser, R. I., Parker, D. S. N., & Mebel, A. M. 2015, *ARPC*, **66**, 43  
Kaiser, R. I., Parker, D. S. N., Zhang, F., et al. 2012, *JPCA*, **116**, 4248  
Kaiser, R. I., Sun, W., Suits, A. G., & Lee, Y. T. 1997, *JCP*, **107**, 8713  
Kislov, V. V., Islamova, N. I., Kolker, A. M., Lin, S. H., & Mebel, A. M. 2005, *JCTC*, **1**, 908  
Kislov, V. V., Nguyen, T. L., Mebel, A. M., Lin, S. H., & Smith, S. C. 2004, *JCP*, **120**, 7008  
Knorke, H., Langer, J., Oomens, J., & Dopfer, O. 2009, *ApJL*, **706**, L66  
Kuan, Y.-J., Yan, C.-H., Charnley, S. B., et al. 2003, *MNRAS*, **345**, 650  
Lee, C., Yang, W., & Parr, R. G. 1988, *PhRvB*, **37**, 785  
Levine, R. D. 2005, *Molecular Reaction Dynamics* (Cambridge: Cambridge Univ. Press)  
Lynch, B. J., & Truhlar, D. G. 2001, *JPCA*, **105**, 2936  
Maity, S., Kaiser, R. I., & Jones, B. M. 2014, *FaDi*, **168**, 485  
Martins, Z., Botta, O., Fogel, M. L., et al. 2008, *E&PSL*, **270**, 130  
Muzangwa, L., Yang, T., Parkar, D. S. N., et al. 2015, *PCCP*, **17**, 7699  
Nuevo, M., Materese, C. K., & Sandford, S. A. 2014, *ApJ*, **793**, 125  
Nuevo, M., Milam, S. N., Sandford, S. A., Elsil, J. E., & Dworkin, J. P. 2009, *Asbio*, **9**, 683  
Parker, D. S. N., Dangi, B. B., Kaiser, R. I., et al. 2014a, *JPCA*, **118**, 12111  
Parker, D. S. N., Dangi, B. B., Kaiser, R. I., et al. 2014b, *JPCA*, **118**, 2709  
Parker, D. S. N., Kaiser, R. I., Kostko, O., et al. 2015, *ApJ*, **803**, 53  
Parker, D. S. N., Yang, T., Kaiser, R. I., Lander, A., & Mebel, A. M. 2014c, *CPL*, **595**, 230  
Parker, D. S. N., Zhang, F., Kim, S. Y., et al. 2012a, *PNAS*, **109**, 53  
Parker, D. S. N., Zhang, F., Kim, Y. S., et al. 2012b, *PCCP*, **14**, 2997  
Peeters, Z., Botta, O., Charnley, S. B., et al. 2005, *A&A*, **433**, 583  
Pizzarello, S., & Holmes, W. 2009, *GeCoA*, **73**, 2150  
Plows, F. L., Elsil, J. E., Zare, R. N., & Buseck, P. R. 2003, *GeCoA*, **67**, 1429  
Puget, J. L., & Leger, A. 1989, *ARA&A*, **27**, 161  
Raghavachari, K., Trucks, G. W., Pople, J. A., & Head-Gordon, M. 1989, *CPL*, **157**, 479  
Ricks, A. M., Douberly, G. E., & Duncan, M. A. 2009, *ApJ*, **702**, 301  
Robins, R. K. 1958, *JACS*, **80**, 6671  
Shao, Y., Molnar, L. F., Jung, Y., et al. 2006, *PCCP*, **8**, 3172  
Smith, K. E., Callahan, M. P., Gerakines, P. A., Dworkin, J. P., & House, C. H. 2014, *GeCoA*, **136**, 1

- Stahl, F., Schleyer, P. v. R., Schaefer, H. F., III, & Kaiser, R. I. 2002, *PISpS*, 50, 685
- Steinfeld, J., Francisco, J., & Hase, W. 1989, *Chemical Kinetics and Dynamics* (Englewood Cliffs, NJ: Prentice Hall)
- Stoks, P. G., & Schwartz, A. W. 1982, *GeCoA*, 46, 309
- Tielens, A. G. G. M. 2008, *ARA&A*, 46, 289
- Tielens, A. G. G. M., van Kerckhoven, C., Peeters, E., & Hony, S. 2000, in *IAU Symp.*, Vol. 197, *Astrochemistry: From Molecular Clouds to Planetary Systems*, ed. Y. C. Minh & E. F. van Dishoeck (San Francisco, CA: ASP), 349
- Turner, B. E. 1971, *ApJL*, 163, L35
- Vernon, M. 1981, PhD Thesis (Berkeley, CA: Univ. California Press)
- Weiss, M. S. 1986, PhD Thesis (Berkeley, CA: Univ. California Press)
- Werner, H.-J., & Knowles, P. J. 2008, MOLPRO version 2008.1, a package of ab initio programs1 (<http://www.molpro.net>)
- Witte, J., Goldey, M., Neaton, J. B., & Head-Gordon, M. 2015, *JCTC*, 11, 1481
- Yang, T., Muzangwa, L., Kaiser, R. I., Jamal, A., & Morokuma, K. 2015, *PCCP*, 17, 21564
- Ziurys, L. M. 2006, *PNAS*, 103, 12274